Physics and Imaging in Radiation Oncology 22 (2022) 20–27

Contents lists available at ScienceDirect

Physics and Imaging in Radiation Oncology

journal homepage: www.sciencedirect.com/journal/physics-and-imaging-in-radiation-oncology

Original Research Article

Extending *in aqua* portal dosimetry with dose inhomogeneity conversion maps for accurate patient dose reconstruction in external beam radiotherapy

Igor Olaciregui-Ruiz [a,*], Julia-Maria Osinga-Blaettermann [b], Karen Ortega-Marin [c], Ben Mijnheer [a], Anton Mans [a]

[a] *Department of Radiation Oncology, The Netherlands Cancer Institute, Plesmanlaan 121, 1066 CX Amsterdam, The Netherlands*
[b] *PTW Freiburg GmbH, Lörracher Straße 7, 79115 Freiburg, Germany*
[c] *Fratoria BV, Rivium 2e straat 22, 2909 LG Capelle aan den IJssel, The Netherlands*

ARTICLE INFO

Keywords:
EPID dosimetry
Back-projection
Monte Carlo dose inhomogeneity conversion
3D dose distribution
VMAT
IMRT

ABSTRACT

Background and purpose: In aqua dosimetry with electronic portal imaging devices (EPIDs) allows for dosimetric treatment verification in external beam radiotherapy by comparing EPID-reconstructed dose distributions (EPID_IA) with dose distributions calculated with the treatment planning system in water-equivalent geometries. The main drawback of the method is the inability to estimate the dose delivered to the patient. In this study, an extension to the method is presented to allow for patient dose reconstruction in the presence of inhomogeneities.
Materials and methods: EPID_IA dose distributions were converted into patient dose distributions (EPID_IA_MC) by applying a 3D dose inhomogeneity conversion, defined as the ratio between patient and water-filled patient dose distributions computed using Monte Carlo calculations. EPID_IA_MC was evaluated against dose distributions calculated with a collapsed cone convolution superposition (CCCS) algorithm and with a GPU-based Monte Carlo dose calculation platform (GPUMCD) using non-transit EPID measurements of 25 plans. *In vivo* EPID measurements of 20 plans were also analyzed.
Results: In the evaluation of EPID_IA_MC, the average γ-mean values (2% local/2mm, 50% isodose volume) were 0.70 ± 0.14 (1SD) and 0.66 ± 0.10 (1SD) against CCCS and GPUMCD, respectively. Percentage differences in median dose to the planning target volume were within 3.9% and 2.7%, respectively. The number of *in vivo* dosimetric alerts with EPID_IA_MC was comparable to EPID_IA.
Conclusions: EPID_IA_MC accommodates accurate patient dose reconstruction for treatment disease sites with significant tissue inhomogeneities within a simple EPID-based direct dose back-projection algorithm, and helps to improve the clinical interpretation of both pre-treatment and *in vivo* dosimetry results.

1. Introduction

Modern external beam radiation therapy demands dosimetric methods to perform patient-specific quality assurance (QA). Electronic portal imaging devices (EPIDs) show dosimetric characteristics [1–4] that have made them suitable for both pre-treatment and *in vivo* dosimetric verification [5–9]. Direct back-projection EPID dosimetry systems use the measured EPID signal to reconstruct dose within the patient model using dose-deposition kernels or other empirically based approaches [10,11]. Our simple direct back-projection algorithm allows for accurate dose reconstruction only in water-equivalent material. In such case, both transit and non-transit EPID dosimetry have proven to be equivalent in dosimetric terms to conventional detector arrays [12]. For dosimetric verification in the presence of inhomogeneities, the *in aqua* method has been developed [13]. In this approach, the algorithm uses the EPID signal to reconstruct dose in a patient-shaped water-equivalent geometry, the so-called water-filled patient. The treatment is verified by comparing EPID-reconstructed dose distributions with dose distributions calculated with the treatment planning system (TPS) in the water-filled patient geometry. The *in aqua* conversion was initially validated with inhomogeneous anthropomorphic phantom measurements in the original paper. The performance of the *in aqua* EPID dosimetry method

* Corresponding author at: Plesmanlaan 121, 1066 CX Amsterdam, The Netherlands.
E-mail address: i.olaciregui@nki.nl (I. Olaciregui-Ruiz).

https://doi.org/10.1016/j.phro.2022.04.001
Received 22 November 2021; Received in revised form 7 April 2022; Accepted 8 April 2022

against TPS dose calculations has been extensively evaluated for non-transit EPID dosimetry [14,15] and for *in vivo* EPID dosimetry [16]. Despite the fact that *in aqua* EPID dosimetry has proven to be useful in detecting variations in patient position and patient anatomy, there are drawbacks inherent to this methodology. First, water-filled patient TPS dose distributions need to be calculated and exported only for EPID dosimetry purposes. This represents additional work for the planning department which, depending on the TPS, may not be easy to streamline. Furthermore, *in aqua* EPID-reconstructed dose distributions do not estimate the actual dose delivered to the patient but the dose delivered to a water-filled patient. Finally, detected deviations cannot easily be related to clinically relevant comparison metrics such as patient dose-volume histograms.

The purpose of this work was to extend *in aqua* EPID dosimetry by incorporating 3D dose inhomogeneity conversion maps, accommodating accurate patient dose reconstruction for treatment disease sites with significant tissue inhomogeneities within a simple EPID-based direct back-projection algorithm. Monte Carlo (MC) dose calculations [17,18] were chosen for the determination of the conversion maps included in this study due to the high accuracy of MC codes in inhomogeneous media [19,20]. The validity of the proposed method was evaluated by comparing EPID-reconstructed dose distributions to reference dose distributions calculated with a collapsed cone convolution superposition algorithm and with a GPU-based MC dose calculation platform. The performance of the method for *in vivo* treatment verification was also investigated.

2. Materials and methods

2.1. EPID measurements and equipment

EPID measurements were made on VersaHD linear accelerators (Elekta, Crawley, UK) equipped with a PerkinElmer XRD 1642 AP amorphous silicon EPID. EPID dose reconstructions were performed with in-house developed clinical software. The EPID dosimetry software reconstructed 3D patient dose distributions for intensity modulated radiation therapy (IMRT) plans and for volumetric modulated arc therapy (VMAT) plans [21]. For IMRT beams, the algorithm used the accumulated image acquired between beam-on and beam-off to reconstruct the dose distribution of the delivered IMRT beam. For VMAT arcs, the algorithm used the sum of all frames acquired within a certain gantry-angle range to reconstruct partial dose distributions, which were summed together to obtain the dose distribution of the delivered VMAT arc. EPID-reconstructed dose distributions of all the beams or arcs were summed together to obtain the EPID-reconstructed dose distribution of the delivered fraction. The grid size for EPID dose reconstructions was 2 mm. Treatment plans were generated with Pinnacle V9.16 (Philips Medical Systems, Eindhoven, The Netherlands). This study was approved by our institutional review board (IRBd20-336).

2.2. Reference dose calculations

Reference dose distributions were calculated with Pinnacle and with a research version of the GPU-based MC dose calculation platform (GPUMCD) developed by Elekta for the Monaco TPS. Pinnacle employs a collapsed cone convolution superposition (CCCS) algorithm [22]. Patient and water-filled patient dose distributions were calculated by turning the inhomogeneity correction on and off in Pinnacle, respectively. Mimicking clinical practice, the grid size for dose calculations was 4 mm for prostate, breast, and lung, 3 mm for head-and-neck and 2 mm for lung stereotactic body radiotherapy (SBRT). GPUMCD employs a GPU-based MC dose calculation algorithm [23]. The MC beam models and machine files required by the algorithm were provided by Elekta. The grid size for dose calculation was 2 mm for all treatment disease sites. For water-filled patient dose calculations, a density override of 1 g/cm^3 was applied to the external contour of the patient.

EPID-reconstructed and reference dose distributions were compared by γ-analysis (2L2 = 2% local/2 mm and 3G2 = 3% global/2mm, 50% isodose volume) and by the percentage difference in the median dose to the planning target volume (PTV) relative to the reference value (ΔPTV_{D50}). 2L2 γ-mean values were used in method evaluation for an estimate of average local dose differences between EPID-reconstructed and reference dose distributions. 3G2 γ-pass rate values were used to investigate the performance of the method for *in vivo* treatment verification. 3G2 was chosen because it is standard clinical practice for IMRT measurement-based QA [24]. In both cases, a threshold value of 50% of the maximum reference dose was selected for γ-analysis because this is the value currently used at our institute for patient-specific dosimetric verification in 3D, both for pre-treatment and *in vivo*. This rather high threshold value is chosen to avoid artificial improvement of the global γ-evaluation results by including low dose volumes.

2.3. Non-transit and transit EPID dosimetry

In the following, we use the notation Xij for a quantity X at pixel ij of the EPID. The back-projection algorithm requires the primary portal dose distribution. In transit mode, $Pr_{ij}^{EPID,transit}$ was calculated from the pixel values $PV_{ij}^{EPID,transit}$ of EPID images and/or frames measured behind the patient or phantom after correcting for the sensitivity matrix S_{ij}, applying the EPID dose response D_R, removing the scatter within the EPID by de-convolving with kernel K_{ij}^{EPID}, correcting for the couch attenuation C_{ij} [25] and removing the scatter SC_{ij}^{EPID} from the patient or phantom to the EPID [10]:

$$Pr_{ij}^{EPID,transit} = ((PV_{ij}^{EPID,transit} \bullet S_{ij} \bullet \mathrm{D_R}) \otimes^{-1} \mathrm{K_{ij}^{EPID}}) \bullet \mathrm{C_{ij}} \bullet \mathrm{SC_{ij}^{EPID}} \quad (1)$$

In non-transit mode, a virtual primary portal dose distribution $Pr_{ij}^{EPID,virtual}$ was estimated using non-transit *in air* EPID measurements and CT data representing the patient anatomy by:

$$Pr_{ij}^{EPID,virtual} = Pr_{ij}^{EPID,inair} \bullet T_{ij}^{CT\_patient} \quad (2)$$

The non-transit *in air* primary portal dose distribution $Pr_{ij}^{EPID,inair}$ was calculated from the pixel values of EPID images and/or frames recorded without the patient in the beam, this time without the corrections for the couch attenuation and the patient scatter. To calculate the primary portal dose transmission $T_{ij}^{CT\_patient}$ from CT data, the radiological thickness of the patient t_{ij}^{radiol}, the linear attenuation coefficient of water for a specific beam energy μ and the beam hardening coefficient σ were used [26]:

$$T_{ij}^{CT\_patient} = e^{-\mu \bullet t_{ij}^{radiol}} + \sigma \bullet \left(t_{ij}^{radiol}\right)^2 \quad (3)$$

The primary portal dose transmission can also be calculated from EPID measurements:

$$T_{ij}^{EPID} = \frac{Pr_{ij}^{EPID,transit}}{Pr_{ij}^{EPID,inair}} \quad (4)$$

The numerical values for μ and σ in Eq. (3) were determined during the commissioning process of the portal dosimetry system by fitting Eq. (3) to Eq. (4) for a set of fields measured with the EPID behind water-equivalent slab-geometry phantoms of different thicknesses. In a situation where the CT data correctly represents the patient anatomy, Eq. (3) and Eq. (4) produce similar results. In such case, the virtual primary portal dose distribution of Eq. (2) becomes an accurate estimate of the transit primary portal dose distribution that would be measured behind the patient in the absence of anatomical changes. The algorithm used Eq. (1) for transit EPID-dosimetry and Eq. (2) for non-transit EPID dosimetry [14].

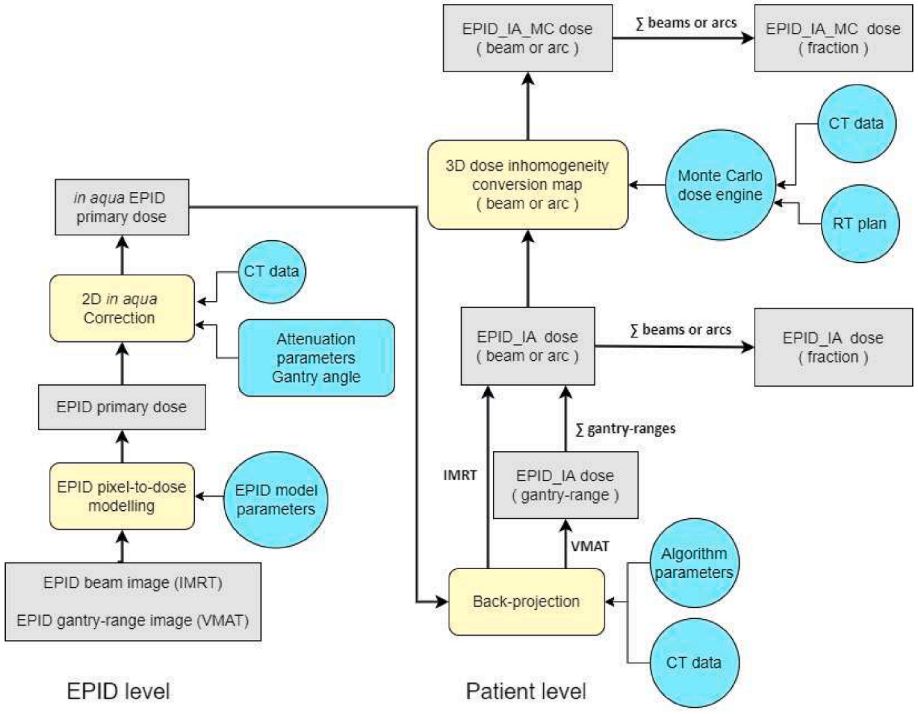

Fig. 1. Schematic diagram of the steps involved in EPID_IA and EPID_IA_MC dose reconstruction. The EPID primary dose is calculated with Eq. (1) for transit EPID dosimetry and with Eq. (2) for non-transit EPID dosimetry.

2.4. EPID dosimetry without correction for inhomogeneities (EPID_NC)

The parameters of the back-projection algorithm were determined during the commissioning process using absolute dose measurements and EPID measurements made behind water-equivalent phantoms. Strictly speaking, if no corrections (NC) are applied for tissue inhomogeneities, the reconstructed dose distributions are accurate only for reconstructions in water-equivalent material and, in transit mode, only if the EPID measurements were made behind water-equivalent phantoms. EPID_NC is used in our clinic for pre-treatment and *in vivo* dosimetric verification of homogeneous treatment disease sites, such as prostate, liver or whole brain.

2.5. In aqua EPID dosimetry (EPID_IA)

The primary portal dose distribution Pr_{ij}^{EPID} was converted into the *in aqua* primary portal dose distribution $Pr_{ij}^{EPID\_IA}$, the equivalent primary portal dose distribution that would be measured behind a water-filled patient by:

$$Pr_{ij}^{EPID\_IA} = Pr_{ij}^{EPID} \bullet \mathrm{IAC_{ij}} = \mathrm{Pr_{ij}^{EPID}} \bullet \frac{\mathrm{T_{ij}^{CT\_water}}}{\mathrm{T_{ij}^{CT\_patient}}} \tag{5}$$

The 2D *in aqua* conversion IAC_{ij} was defined as the ratio between two primary portal transmission images calculated from the water-patient and patient CT scan, respectively. For non-transit dosimetry, the *in aqua* primary portal dose distribution estimates the transit primary portal dose distribution that would be measured behind the water-filled patient in the absence of anatomical changes:

$$Pr_{ij}^{EPID\_IA,non-transit} = Pr_{ij}^{EPID,virtual} \bullet \frac{T_{ij}^{CT\_water}}{T_{ij}^{CT\_patient}} = Pr_{ij}^{EPID,in\_air} \bullet \mathrm{T_{ij}^{CT\_water}} \tag{6}$$

For transit EPID dosimetry, the effect of the *in aqua* conversion is to 'remove' the effect that patient inhomogeneities have on the primary portal dose distribution.

$$Pr_{ij}^{EPID\_IA,transit} = Pr_{ij}^{EPID,transit} \bullet \frac{\mathrm{T_{ij}^{CT\_water}}}{\mathrm{T_{ij}^{CT\_patient}}} \tag{7}$$

The *in aqua* conversion is accurate only if the CT scan perfectly accounts for the anatomy of the patient during the delivery. Otherwise, as often is the case with transit *in vivo* measurements, the *in aqua* conversion helps to determine a change in the delivery from the planned delivery. The algorithm used Eq. (6) for non-transit *in aqua* EPID dosimetry and Eq. (7) for transit *in aqua* EPID dosimetry. EPID_IA is used in our clinic for pre-treatment and *in vivo* dosimetric verification of treatment disease sites involving large tissue inhomogeneities, such as lung.

2.6. In aqua EPID dosimetry with Monte Carlo dose inhomogeneity conversion (EPID_IA_MC)

For each IMRT beam or VMAT arc, EPID_IA dose distributions D^{EPID_IA} calculated in the water-filled patient were converted into patient dose distributions $D^{EPID\_IA\_MC}$ by applying a voxel-by-voxel 3D dose inhomogeneity conversion DIC^{MC}:

$$D^{EPID\_IA\_MC} = D^{EPID\_IA} \bullet \mathrm{DIC^{MC}} = \mathrm{D^{EPID\_IA}} \bullet \frac{\mathrm{D^{MC\_patient}}}{\mathrm{D^{MC\_water}}} \tag{8}$$

The conversion was defined as the ratio between patient and water-filled patient MC dose distributions. EPID_IA_MC dose distributions of all beams or arcs were summed together to obtain the EPID_IA_MC dose distribution of the delivered fraction. Fig. 1. displays a schematic diagram of the steps involved in EPID_IA and EPID_IA_MC dose reconstruction.

The SciMoCa dose engine (ScientificRT GmbH, Munich, Germany) was used for DIC^{MC} calculations using a dose grid size of 2 mm [27,28]. The CT number to mass density conversion map was set equal to the one used in our TPS. For water-filled patient dose calculations, a density override of 1 g/cm^3 was applied to the external contour of the patient. The nominal dose computation uncertainty in SciMoCa can be selected from six options: Extra Fast (4%), Fast (2%), Fine (1%), Extra Fine

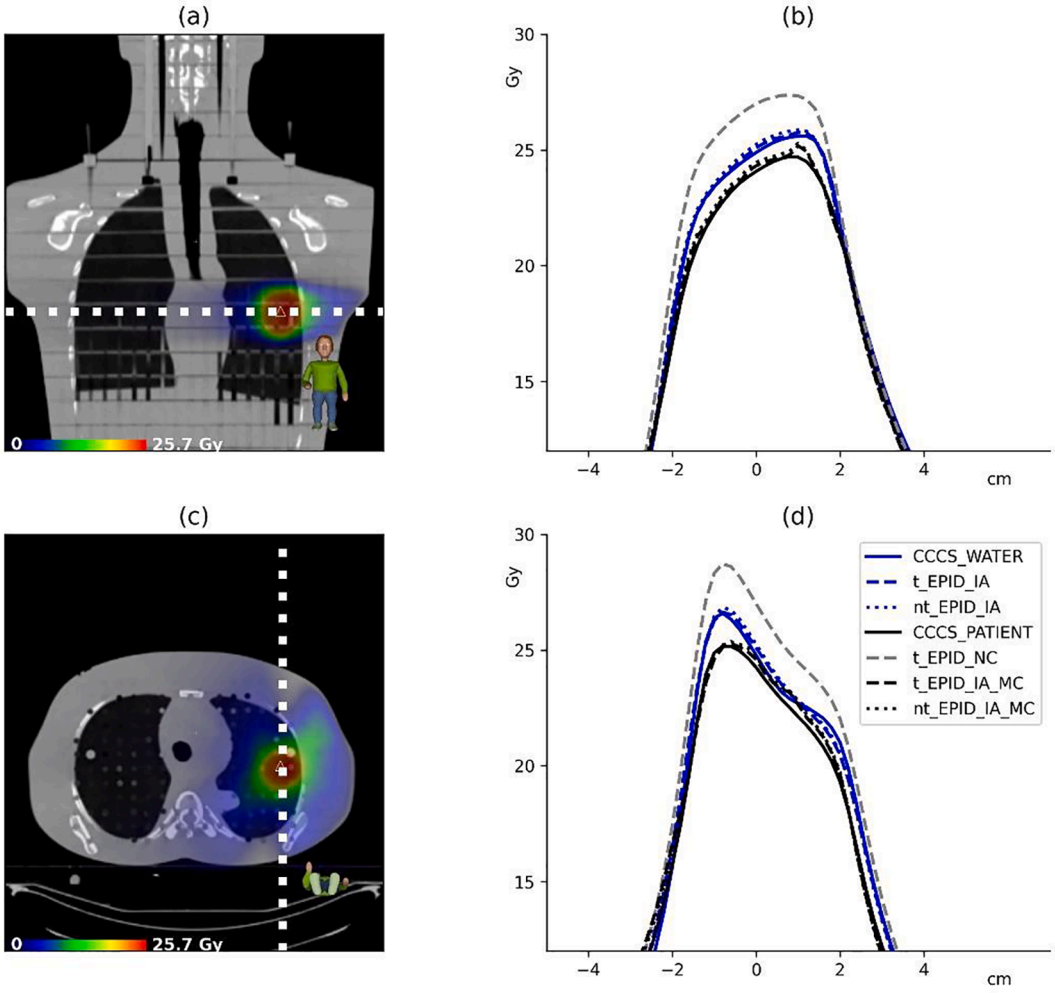

Fig. 2. CT scan of the anthropomorphic (Alderson) phantom and TPS-calculated dose distribution for a double-arc VMAT lung plan in (a) coronal view and (c) axial view, dose profiles through the isocentre in the (b) left–right and (d) anterior-posterior directions. EPID dose reconstructions were performed in three back-projection modes: without corrections (EPID_NC), *in aqua* (EPID_IA) and *in aqua* combined with Monte Carlo dose inhomogeneities conversion maps determined with Scimoca dose calculations (EPID_IA_MC). nt_EPID and t_EPID refer to non-transit and transit EPID dosimetry, respectively. CCCS_PATIENT and CCCS_WATER refer to dose calculations performed with a collapsed cone convolution superposition algorithm for the patient and water-filled patient geometries, respectively.

(0.5%), Commissioning (0.25%) and Ultimate (0.1%). Such nominal uncertainty is defined as the average uncertainty for voxels with a dose larger than 70% of the maximum dose. In a preliminary investigation with three patient cases, an uncertainty of 0.5% showed the best compromise between accuracy and computation times. Calculations were performed in an Oracle Linux 7.6 server with an Intel Xeon E5-2697A v4 CPU (64 logical cores @ 2.60 GHz) and a 125 GB RAM. The average calculation time was 2.2 ± 1.8(1SD) minutes. 6 MV (FF) and 10 MV (FF and FFF) photon beams were included in this study. MC beam models based on Elekta's standard beam data for Versa HD linacs were used for dose calculations.

2.7. Alderson phantom measurements

An inhomogeneous anthropomorphic (Alderson) phantom was used to mimic *in vivo* patient dose reconstruction as much as possible. The Alderson phantom was irradiated using a double arc VMAT lung plan. Non-transit and transit EPID measurements were performed to reconstruct EPID_NC, EPID_IA and EPID_IA_MC dose distributions.

2.8. Evaluation of EPID_IA_MC dosimetry

Non-transit *in air* EPID measurements for 20 double arc VMAT plans (5 prostate, 5 head-and-neck, 5 lung and 5 lung SBRT) and for 5 IMRT breast plans were used to reconstruct EPID_NC, EPID_IA and EPID_IA_MC dose distributions. *In air* non-transit EPID dose reconstructions to the patient anatomy were used for method evaluation because they are exempt of patient related deviations.

2.9. In vivo treatment verification with EPID_IA_MC dosimetry

In vivo EPID measurements for plans of three treatment disease sites involving large inhomogeneities were evaluated: 18 VMAT lung fractions (9 plans), 16 VMAT lung SBRT fractions (8 plans) and 9 IMRT breast fractions (3 plans). IMRT dose reconstruction for breast plans was performed using the primary portal dose transmission calculated from EPID measurements as given in Eq. (4). In vivo dosimetry systems act as binary classifiers where plans are classified either as fail (alerted) or pass (non-alerted). The performance of EPID_IA and EPID_IA_MC regarding alert classification was compared by calculating the percentage of passing plans with varying alert threshold values for γ-pass rate results.

Table 1
Comparison between non-transit EPID-reconstructed and reference 3D dose distributions using 2L2 γ-analysis and ΔPTV_{D50}. EPID_IA distributions were compared to reference dose distributions calculated in the water-filled patient. 20 double arc VMAT plans (5 prostate, 5 head-and-neck, 5 lung and 5 lung SBRT) and 5 IMRT breast plans were analyzed. Results are presented as average±(1SD). The last row presents the average results for all treatment disease sites together with the range displayed between parenthesis.

	2L2 γ-mean			ΔPTV_{D50} (%)		
	EPID_NC	EPID_IA	EPID_IA_MC	EPID_NC	EPID_IA	EPID_IA_MC
vs CCCS						
Prostate	0.53 ± 0.12	0.57 ± 0.04	0.53 ± 0.05	1.0 ± 0.9	−0.5 ± 1.1	−0.1 ± 0.9
Head-and-neck	0.70 ± 0.08	0.71 ± 0.11	0.75 ± 0.10	−0.8 ± 0.8	−1.2 ± 0.8	−1.5 ± 0.6
Breast	1.48 ± 1.03	0.72 ± 0.11	0.78 ± 0.12	1.5 ± 2.7	−0.6 ± 1.4	−0.5 ± 1.5
Lung	2.33 ± 0.95	0.71 ± 0.04	0.83 ± 0.07	6.7 ± 6.4	0.8 ± 1.0	0.8 ± 1.8
Lung SBRT	4.17 ± 0.91	0.59 ± 0.04	0.61 ± 0.09	32.5 ± 9.5	1.3 ± 0.9	−0.1 ± 3.0
Total		0.66 ± 0.10 (0.52, 0.86)	0.70 ± 0.14 (0.49, 0.93)		0.0 ± 1.5 (-2.2, 2.8)	−0.3 ± 1.8 (-3.6, 3.9)
vs GPUMCD						
Prostate	0.56 ± 0.10	0.54 ± 0.06	0.55 ± 0.05	0.9 ± 0.9	−0.5 ± 0.9	−0.1 ± 1.3
Head-and-neck	0.70 ± 0.04	0.69 ± 0.05	0.72 ± 0.05	0.1 ± 0.9	−0.7 ± 0.6	−0.6 ± 0.6
Breast	1.53 ± 0.96	0.72 ± 0.09	0.72 ± 0.08	2.3 ± 2.5	0.0 ± 0.9	−0.1 ± 1.3
Lung	1.88 ± 0.81	0.64 ± 0.10	0.72 ± 0.08	6.0 ± 5.7	−0.2 ± 0.5	−0.7 ± 0.6
Lung SBRT	3.76 ± 1.30	0.60 ± 0.03	0.57 ± 0.03	29.0 ± 15.8	1.0 ± 1.1	0.6 ± 1.1
Total		0.64 ± 0.09 (0.49, 0.82)	0.66 ± 0.10 (0.49, 0.83)		0.0 ± 1.1 (-1.7, 2.8)	−0.3 ± 1.2 (-2.7, 2.0)

EPID_NC = EPID dosimetry with No Correction.
EPID_IA = In Aqua EPID dosimetry.
EPID_IA_MC = In Aqua EPID dosimetry with Monte Carlo based dose inhomogeneity correction maps.
CCCS = Collapse Cone Convolution Superposition algorithm.
GPUMCD = GPU-based Monte Carlo Dose calculation algorithm.

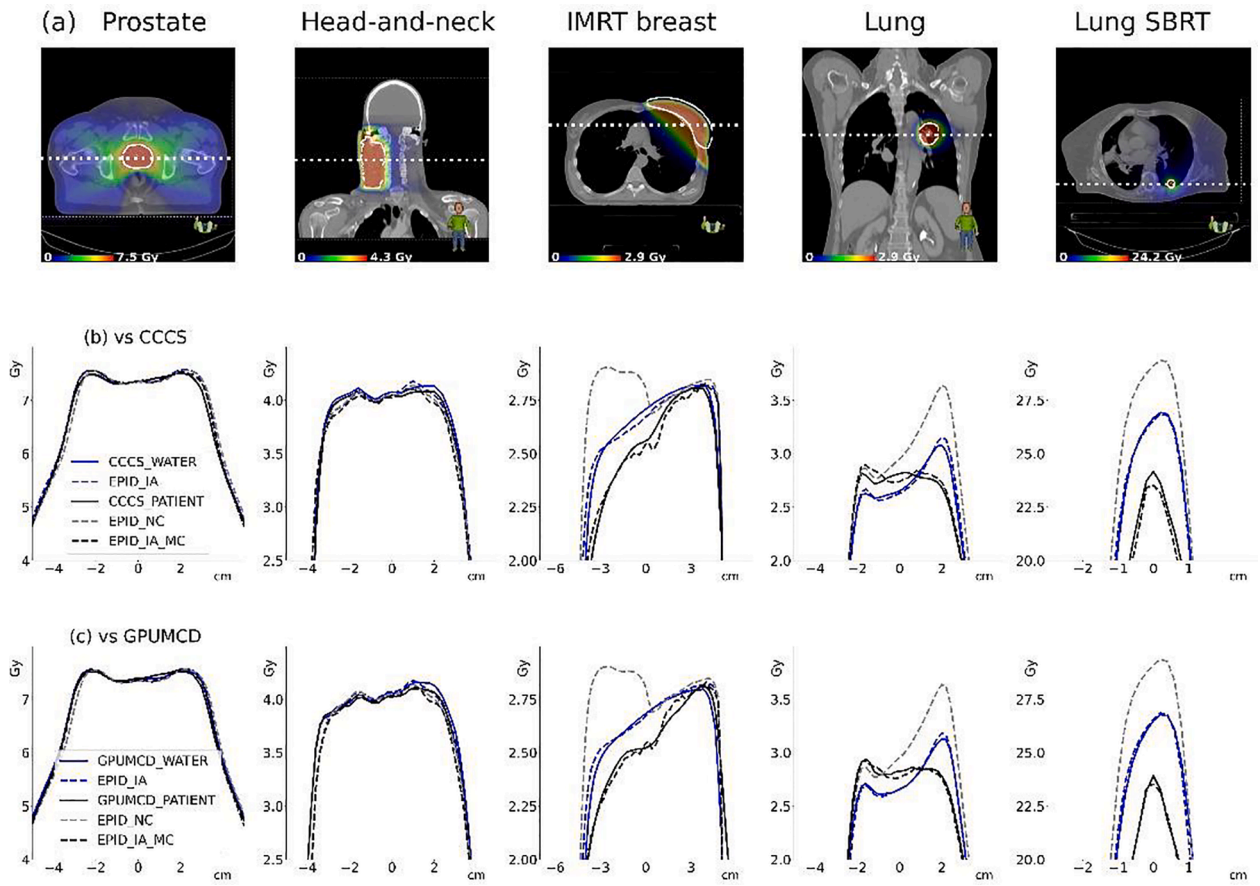

Fig. 3. (a) TPS-calculated dose distributions for five plans of different treatment disease sites, EPID-reconstructed left–right dose profiles through the center of the PTV compared to dose profiles calculated with (b) a collapsed cone convolution superposition algorithm (CCCS) and with (c) a GPU-based Monte Carlo dose calculation algorithm (GPUMCD). EPID dose reconstructions were performed with non-transit EPID measurements in three back-projection modes: without corrections (EPID_NC), *in aqua* (EPID_IA) and *in aqua* combined with Monte Carlo dose inhomogeneities conversion maps determined with SciMoCa dose calculations (EPID_IA_MC). CCCS_PATIENT and CCCS_WATER refer to dose calculations performed with CCCS for the patient and water-filled patient geometries, respectively. GPUMCD_PATIENT and GPUMCD _WATER refer to dose calculations performed with GPUMCD for the patient and water-filled patient geometries, respectively.

Table 2
Comparison between *in vivo* EPID-reconstructed and reference 3D dose distributions for plans of three treatment disease sites involving large inhomogeneities using 3G2 γ-analysis and ΔPTV_{D50}. EPID_IA distributions were compared to reference dose distributions calculated in the water-filled patient. 18 VMAT lung fractions (9 plans), 16 VMAT lung SBRT fractions (8 plans) and 9 IMRT breast fractions (3 plans) were analyzed. γ-pass rate results are presented as median (interquartile range). ΔPTV_{D50} results are presented as average ±(1SD). The last row presents average results for all treatment disease sites together with the ΔPTV_{D50} range indicated between parenthesis.

	3G2 γ-pass rate (%)		ΔPTV_{D50} (%)	
	EPID_IA	EPID_IA_MC	EPID_IA	EPID_IA_MC
vs CCCS				
Breast	92.7 (5.0)	90.0 (3.1)	−0.6 ± 0.9	−0.3 ± 1.3
Lung	94.5 (3.2)	90.7 (4.3)	0.2 ± 1.4	0.3 ± 1.5
Lung SBRT	99.3 (0.8)	98.9 (4.1)	1.5 ± 1.5	1.0 ± 2.8
Total	95.2 (5.6)	91.9 (7.1)	0.5 ± 1.5 (−2.2, 4.0)	0.4 ± 2.1 (−3.4, 6.5)
vs GPUMCD				
Breast	91.4 (3.1)	92.5 (4.1)	0.3 ± 1.6	0.1 ± 1.3
Lung	96.0 (2.7)	93.5 (3.1)	−0.9 ± 1.7	−1.1 ± 1.7
Lung SBRT	99.3 (1.4)	99.7 (1.0)	0.8 ± 1.9	−0.3 ± 2.2
Total	96.9 (4.9)	95.7 (6.4)	0.1 ± 1.9 (−4.1, 4.2)	−0.5 ± 1.9 (−4.3, 3.3)

EPID_IA = In Aqua EPID dosimetry.
EPID_IA_MC = In Aqua EPID dosimetry with Monte Carlo based dose inhomogeneity correction maps.
CCCS = Collapse Cone Convolution Superposition algorithm.
GPUMCD = GPU-based Monte Carlo Dose calculation algorithm.

3. Results

3.1. Alderson phantom measurements

In the 2L2 γ-comparison against CCCS-calculated patient dose distributions, γ-mean values of 0.58 and 0.56 were found for transit and non-transit EPID_IA_MC dosimetry, respectively. ΔPTV_{D50} results were within 1.5%. As can be seen in the dose profiles presented in Fig. 2, the transit and non-transit EPID_IA_MC dosimetry distributions were nearly identical and agreed well with the patient reference dose distribution. Compared with each other, the 2L2 γ-mean value was 0.3 and the ΔPTV_{D50} value was 0.1%.

3.2. Evaluation of EPID_IA_MC dosimetry

In the comparison of EPID_IA with reference water-filled patient dose calculations, 2L2 γ-mean values were lower or equal to 0.86 and ΔPTV_{D50} deviations were within 2.8% (see Table 1). In the comparison of EPID_IA_MC with reference patient dose calculations, 2L2 γ-mean values were lower or equal to 0.93 and ΔPTV_{D50} deviations were within 3.9%. The EPID_IA_MC agreement was better against GPUMCD than against CCCS. The differences between EPID_IA_MC and EPID_IA results are explained by the extra discrepancies between the algorithm employed in the calculation of the DIC^{MC} conversion (SciMoCa) and in the computation of the reference dose distribution (CCCS and GPUMCD). These differences were small for prostate and head-and-neck but they became larger for treatment disease sites with significant tissue inhomogeneities. For lung, the average increase in 2L2 γ-mean values was 0.12 ± 0.07(1SD) against CCCS and 0.08 ± 0.03(1SD) against GPUMCD. For lung SBRT, the average differences in ΔPTV_{D50} results were −1.4% ± 3.1%(1SD) and −0.4% ± 1.0%(1SD), respectively. For illustration purposes, Fig. 3 exhibits results for arbitrarily selected plans of five treatment disease sites. For completeness EPID_NC results are also displayed.

3.3. In vivo treatment verification with EPID_IA_MC dosimetry

For the *in vivo* treatment verification cases, the EPID_IA_MC agreement was again better against GPUMCD than against CCCS (see Table 2). Differences between EPID_IA_MC and EPID_IA results were also observed. For all treatment disease sites together, the average decrease in 3G2 γ-pass rate values was 2.5% ± 2.5%(1SD) against CCCS and 0.8% ± 2.2%(1SD) against GPUMCD. These differences explain the somewhat lower percentage of passing plans with EPID_IA_MC than with EPID_IA, see Fig. 4.

4. Discussion

In this study, we have extended the *in aqua* EPID dosimetry method by incorporating a MC-based dose inhomogeneity conversion map. This was illustrated with the examples of Fig. 3 where EPID_IA water-filled patient dose distributions were converted into EPID_IA_MC patient dose distributions that can be compared with reference patient dose calculations, therefore improving the clinical interpretation of results.

In this study, non-transit EPID_IA_MC dosimetry was evaluated against dose calculations performed with CCCS and GPUMCD algo-

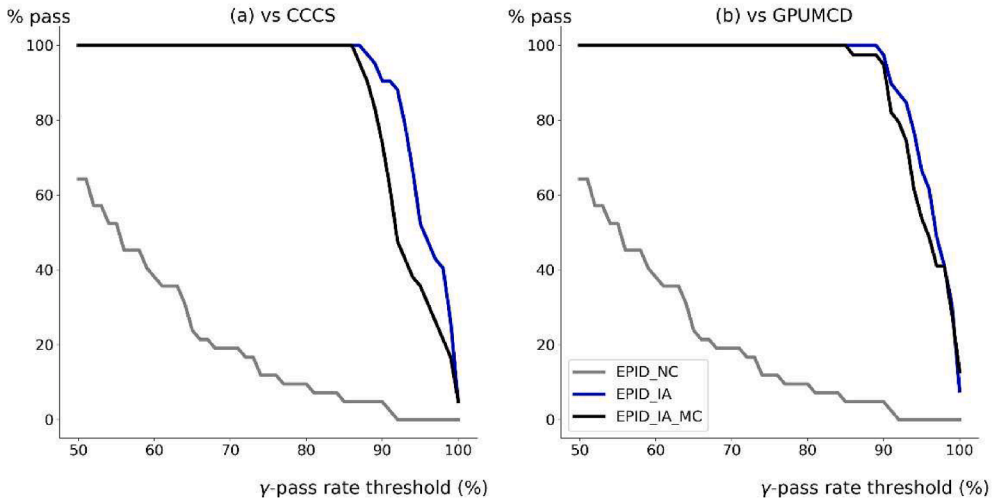

Fig. 4. In vivo *p*ercentage of passing plans (% pass) with varying alert threshold values for 3G2 γ-pass rate results for plans of three treatment disease sites involving large inhomogeneities. Results corresponding to 18 VMAT lung fractions (9 plans), 16 VMAT lung SBRT fractions (8 plans) and 9 IMRT breast fractions (3 plans) were included. EPID dose reconstructions were performed in two back-projection modes: *in aqua* (EPID_IA) and *in aqua* combined with Monte Carlo conversion maps determined with SciMoCa dose calculations (EPID_IA_MC). Results were presented using reference dose distributions calculated with (a) a collapsed cone convolution superposition algorithm (CCCS) and with (b) a GPU-based Monte Carlo dose calculation algorithm (GPUMCD).

rithms (see Table 1). The largest 2L2 γ-mean value was 0.93. This suggests that, for the worst case, an average dose difference of ~ 2% is expected in low-dose gradient regions or a distance-to-agreement of 2 mm in steep gradient region which is considered adequate for the purpose of EPID-based pre-treatment verification. A similar evaluation of transit EPID_IA_MC dosimetry with EPID measurements made behind anthropomorphic phantoms was deemed unnecessary for this study. The reason is that transit and non-transit EPID_IA dosimetry produce nearly identical results in such case. The underlying principle of non-transit EPID dosimetry is that $Pr_{ij}^{EPID,virtual}$ correctly estimates $Pr_{ij}^{EPID,transit}$ in the absence of anatomical changes. Note how, in that situation, Eq. (7) becomes effectively Eq. (6). In other words, an 'evaluation' of non-transit EPID dosimetry implicitly 'evaluates' transit EPID dosimetry for phantom measurements. This was confirmed by the excellent agreement between transit and non-transit EPID_IA dosimetry with measurements made for a VMAT lung plan behind the Alderson phantom (see Fig. 1). With respect to the performance of EPID_IA_MC for *in vivo* treatment verification, the introduction of EPID_IA_MC would lead to a decrease in the number of passing plans compared to EPID_IA. Fig. 4 exhibited how the extent of the decrease depends on the algorithms employed for the calculation of the DIC^{MC} conversion and for the reference dose distribution. The more similar these algorithms are to each other, the more closely the EPID_IA and EPID_IA_MC verification results are related.

In indirect EPID back-projection methods, the EPID signal is back-projected through the patient model to determine the incident fluence to the patient. This fluence, together with a patient model, is fed into a conventional forward dose engine to calculate the contribution of each EPID image (frame) to the total patient dose distribution [29–31]. EPID_IA_MC results compare well with indirect back-projection methods [32,33]. The clear advantage of EPID_IA_MC over indirect methods is the extremely fast direct back-projection calculation times of around 100 ms provided that all inputs to the algorithm that are EPID-independent are precomputed [34]. In a clinical setting, one would expect DIC^{MC} to be precomputed automatically, which is essential for a large-scale clinical implementation [35]. In conventional workflows, DIC^{MC} would be computed using the reference RT plan and the planning CT. In online adaptive workflows, DIC^{MC} would be computed using the online adapted RT plan and the daily CT scan.

In conclusion, EPID_IA_MC accommodates accurate patient dose reconstruction for treatment disease sites with significant tissue inhomogeneities within a simple EPID-based direct dose back-projection algorithm, and helps to improve the clinical interpretation of *in vivo* dosimetry results.

Declaration of Competing Interest

The authors declare the following financial interests/personal relationships which may be considered as potential competing interests: Igor Olaciregui-Ruiz, Ben Mijnheer and Anton Mans declare that their department collaborates with PTW (Freiburg, Germany) for the development of portal dosimetry products. Julia-Maria Osinga-Blättermann is employee of PTW and Karen Ortega-Marin is employee of Fratoria (Capelle aan den IJssel, The Netherlands).

Acknowledgements

The authors would like to thank Javier Salguero, Vijaya Ambati and Iaroslav Smychliaev from Fratoria for providing infrastructure and support to perform SciMoCa dose calculations and Jan Weidner and Oliver Schrenk from PTW for fruitful discussions. The authors would like to thank Elekta for providing the research version of the GPUMCD algorithm.

References

[1] Greer PB, Popescu CC. Dosimetric properties of an amorphous silicon electronic portal imaging device for verification of dynamic intensity modulated radiation therapy. Med Phys 2003;30:1618–27. https://doi.org/10.1118/1.1582469.
[2] Greer PB. Correction of pixel sensitivity variation and off-axis response for amorphous silicon EPID dosimetry. Med Phys 2005;32:3558–68. https://doi.org/10.1118/1.2128498.
[3] Winkler P, Hefner A, Georg D. Dose-response characteristics of an amorphous silicon EPID. Med Phys 2005;32:3095–105. https://doi.org/10.1118/1.2040711.
[4] McDermott LN, Louwe RJW, Sonke J-J, van Herk MB, Mijnheer BJ. Dose–response and ghosting effects of an amorphous silicon electronic portal imaging device. Med Phys 2004;31:285–95. https://doi.org/10.1118/1.1637969.
[5] van Elmpt W, McDermott L, Nijsten S, Wendling M, Lambin P, Mijnheer B. A literature review of electronic portal imaging for radiotherapy dosimetry. Radiother Oncol 2008;88:289–309. https://doi.org/10.1016/j.radonc.2008.07.008.
[6] McCurdy B, Greer P, Bedford J. Electronic Portal Imaging Device Dosimetry. In: Mijnheer B, editor. Clinical 3D Dosimetry in modern radiation therapy. Boca Raton, FL: CRC Press; 2017. p. 169–98.
[7] Mijnheer BJ, González P, Olaciregui-Ruiz I, Rozendaal RA, van Herk M, Mans A. Overview of 3-year experience with large-scale electronic portal imaging device-based 3-dimensional transit dosimetry. Pract Radiat Oncol 2015;5:e679–87. https://doi.org/10.1016/j.prro.2015.07.001.
[8] Bossuyt E, Weytjens R, Nevens D, De Vos S, Verellen D. Evaluation of automated pre-treatment and transit in-vivo dosimetry in radiotherapy using empirically determined parameters. Phys Imaging Radiat Oncol 2020;16:113–29. https://doi.org/10.1016/j.phro.2020.09.011.
[9] Olaciregui-Ruiz I, Beddar S, Greer P, Jornet N, McCurdy B, Paiva-Fonseca G, et al. In vivo dosimetry in external beam photon radiotherapy: Requirements and future directions for research, development, and clinical practice. Phys Imaging Radiat Oncol 2020;15:108–16. https://doi.org/10.1016/j.phro.2020.08.003.
[10] Wendling M, Louwe RJW, McDermott LN, Sonke J-J, van Herk M, Mijnheer BJ. Accurate two-dimensional IMRT verification using a back-projection EPID dosimetry method. Med Phys 2006;33:259–73. https://doi.org/10.1118/1.2147744.
[11] Wendling M, McDermott LN, Mans A, Sonke J-J, van Herk M, Mijnheer BJ. A simple backprojection algorithm for 3D in vivo EPID dosimetry of IMRT treatments. Med Phys 2009;36:3310–21. https://doi.org/10.1118/1.3148482.
[12] Olaciregui-Ruiz I, Vivas-Maiques B, Kaas J, Perik T, Wittkamper F, Mijnheer B, et al. Transit and non-transit 3D EPID dosimetry versus detector arrays for patient specific QA. J Appl Clin Med Phys 2019;20:79–90. https://doi.org/10.1002/acm2.12610.
[13] Wendling M, McDermott LN, Mans A, Olaciregui-Ruiz Í, Pecharromán-Gallego R, Sonke J-J, et al. In aqua vivo EPID dosimetry. Med Phys 2012;39:367–77. https://doi.org/10.1118/1.3665709.
[14] Olaciregui-Ruiz I, Rozendaal R, van Oers RFM, Mijnheer B, Mans A. Virtual patient 3D dose reconstruction using in air EPID measurements and a back-projection algorithm for IMRT and VMAT treatments. Phys Medica 2017;37:49–57. https://doi.org/10.1016/j.ejmp.2017.04.016.
[15] Olaciregui-Ruiz I, Rozendaal R, Mijnheer B, Mans A. Site-specific alert criteria to detect patient-related errors with 3D EPID transit dosimetry. Med Phys 2019;46:45–55. https://doi.org/10.1002/mp.13265.
[16] Sterckx B, Steinseifer I, Wendling M. In vivo dosimetry with an electronic portal imaging device for prostate cancer radiotherapy with an endorectal balloon. Phys Imaging Radiat Oncol 2019;12:7–9. https://doi.org/10.1016/j.phro.2019.10.002.
[17] Brualla L, Rodriguez M, Lallena AM. Monte Carlo systems used for treatment planning and dose verification. Strahlenther Onkol 2017;193:243–59. https://doi.org/10.1007/s00066-016-1075-8.
[18] Andreo P. Monte Carlo simulations in radiotherapy dosimetry. Radiat Oncol 2018;13:121. https://doi.org/10.1186/s13014-018-1065-3.
[19] Papanikolaou N, Stathakis S. Dose-calculation algorithms in the context of inhomogeneity corrections for high energy photon beams. Med Phys 2009;36:4765–75. https://doi.org/10.1118/1.3213523.
[20] Kry SF, Alvarez P, Molineu A, Amador C, Galvin J, Followill DS. Algorithms used in heterogeneous dose calculations show systematic differences as measured with the radiological physics center's anthropomorphic thorax phantom used for RTOG credentialing. Int J Radiat Oncol Biol Phys 2013;85:e95–100. https://doi.org/10.1016/j.ijrobp.2012.08.039.
[21] Mans A, Remeijer P, Olaciregui-Ruiz I, Wendling M, Sonke J-J, Mijnheer B, et al. 3D Dosimetric verification of volumetric-modulated arc therapy by portal dosimetry. Radiother Oncol 2010;94:181–7. https://doi.org/10.1016/j.radonc.2009.12.020.
[22] Ahnesjö A. Collapsed cone convolution of radiant energy for photon dose calculation in heterogeneous media. Med Phys 1989;16:577–92. https://doi.org/10.1118/1.596360.
[23] Paudel MR, Kim A, Sarfehnia A, Ahmad SB, Beachey DJ, Sahgal A, et al. Experimental evaluation of a GPU-based monte carlo dose calculation algorithm in the Monaco treatment planning system. J Appl Clin Med Phys 2016;17:230–41. https://doi.org/10.1120/jacmp.v17i6.6455.
[24] Miften M, Olch A, Mihailidis D, Moran J, Pawlicki T, Molineu A, et al. Tolerance limits and methodologies for IMRT measurement-based verification QA: Recommendations of AAPM Task Group No. 218. Med Phys 2018;45:e53–83. https://doi.org/10.1002/mp.12810.

[25] Olaciregui-Ruiz I, Rozendaal R, Mijnheer B, Mans A. A 2D couch attenuation model for in vivo EPID transit dosimetry. Biomed Phys Eng Express 2018;4(025027). https://doi.org/10.1088/2057-1976/aaa370.
[26] Pecharromán-Gallego R, Mans A, Sonke J-J, Stroom JC, Olaciregui-Ruiz I, Van Herk M, et al. Simplifying EPID dosimetry for IMRT treatment verification. Med Phys 2011;38. https://doi.org/10.1118/1.3547714.
[27] Piffer S, Casati M, Marrazzo L, Arilli C, Calusi S, Desideri I, et al. Validation of a secondary dose check tool against Monte Carlo and analytical clinical dose calculation algorithms in VMAT. J Appl Clin Med Phys 2021;22:52–62. https://doi.org/10.1002/acm2.13209.
[28] Hoffmann L, Alber M, Söhn M, Elstrøm UV. Validation of the Acuros XB dose calculation algorithm versus Monte Carlo for clinical treatment plans. Med Phys 2018;45:3909–15. https://doi.org/10.1002/mp.13053.
[29] van Elmpt W, Nijsten S, Petit S, Mijnheer B, Lambin P, Dekker A. 3D In Vivo Dosimetry Using Megavoltage Cone-Beam CT and EPID Dosimetry. Int J Radiat Oncol Biol Phys 2009;73:1580–7. https://doi.org/10.1016/j.ijrobp.2008.11.051.
[30] Van Uytven E, Van Beek T, McCowan PM, Chytyk-Praznik K, Greer PB, McCurdy BMC. Validation of a method for in vivo 3D dose reconstruction for IMRT and VMAT treatments using on-treatment EPID images and a model-based forward-calculation algorithm. Med Phys 2015;42:6945–54. https://doi.org/10.1118/1.4935199.
[31] McCowan PM, Asuni G, Van Uytven E, VanBeek T, McCurdy BMC, Loewen SK, et al. Clinical Implementation of a Model-Based In Vivo Dose Verification System for Stereotactic Body Radiation Therapy-Volumetric Modulated Arc Therapy Treatments Using the Electronic Portal Imaging Device. Int J Radiat Oncol Biol Phys 2017;97:1077–84. https://doi.org/10.1016/j.ijrobp.2017.01.227.
[32] McCowan PM, Asuni G, Van Beek T, Van Uytven E, Kujanpaa K, McCurdy BMC. A model-based 3D patient-specific pre-treatment QA method for VMAT using the EPID. Phys Med Biol 2017;62:1600–12. https://doi.org/10.1088/1361-6560/aa590a.
[33] Narayanasamy G, Zalman T, Ha CS, Papanikolaou N, Stathakis S. Evaluation of Dosimetry Check software for IMRT patient-specific quality assurance. J Appl Clin Med Phys 2015;16:329–38. https://doi.org/10.1120/jacmp.v16i3.5427.
[34] Spreeuw H, Rozendaal R, Olaciregui-Ruiz I, González P, Mans A, Mijnheer B, et al. Online 3D EPID-based dose verification: Proof of concept. Med Phys 2016;43 (3969–74). https://doi.org/10.1118/1.4952729.
[35] Olaciregui-Ruiz I, Rozendaal R, Mijnheer B, van Herk M, Mans A. Automatic in vivo portal dosimetry of all treatments. Phys Med Biol 2013;58:8253–64. https://doi.org/10.1088/0031-9155/58/22/8253.